First-principles time-dependent quantum transport theory

Yu Zhang, Shuguang Chen, and GuanHua Chen*
Department of Chemistry, The University of Hong Kong, Hong Kong, China
(Received 21 December 2012; published 8 February 2013)

A practical first-principles scheme for time-dependent transport through realistic systems at finite temperature is established by the combination of time-dependent density functional theory and nonequilibrium Green's-function formalism with wide-band limit approximation. This method extends the adiabatic wide-band limit approximation developed earlier [Zheng *et al*., Phys. Rev. B **75**, 195127 (2007)]. It is implemented with both time-dependent density functional theory and time-dependent density functional tight-binding method and is applied to simulate the time-dependent transport through a carbon nanotube based electronic device to demonstrate its validity.

DOI: 10.1103/PhysRevB.87.085110 PACS number(s): 71.15.Mb, 72.10.Bg, 73.23.Ad, 73.63.−b

I. INTRODUCTION

First-principles method for the open quantum system has seen a tremendous growth of research interest.[1–7] Based on the time-dependent holographic electron-density theorem, the existence of rigorous first-principles method for open electronic system was confirmed.[1,8] Consequently, time-dependent density functional theory (TDDFT)[9] was combined with nonequilibrium Green's function (NEGF) method to study the time-dependent quantum transport and was termed as TDDFT-NEGF.[1,8,10–17] If current density is employed as the basic physical quantity of interest, the extension of time-dependent current-density functional theory (TDCDFT)[18] to open quantum system was rigorously established, which was termed as stochastic TDCDFT.[2,3] Based on TDDFT-NEGF, practical numerical schemes were developed in terms of the equation of motion (EOM) for the reduced single-electron density matrix (RSDM).[1,8] Within the TDDFT-NEGF theory, the RSDM was integrated in time-domain,[1] and the resulting TDDFT-NEGF-EOM was solved to investigate the transient current through carbon nanotube (CNT) based device under both ac and dc bias voltages. It was found that the transient electronic dynamic of the CNT-based device can be understood in terms of equivalent classical circuit.[19] In these calculations, the adiabatic wide-band limit (AWBL) approximation was employed to account for the dissipative interaction between the device and the environment. The AWBL is valid for zero temperature, and is expected to be only suitable for low-frequency response. In order to capture the ultrafast process and deal with the systems at finite temperature, a more accurate method is desired. Among many methods,[6,11–13] the hierarchical equation of motion (HEOM) is a promising candidate to account for the dissipative interaction between the device and environment.[12,14] Combined with TDDFT, the resulting TDDFT-NEGF-HEOM terminates at the second tier.[12,14] Unfortunately, this two-tier-HEOM is not efficient for the simulation of realistic devices. However, when the wide-band limit (WBL) approximation is adopted, the resulting TDDFT-NEGF-HEOM-WBL terminates at the first tier, making the overall method much more efficient. In this paper, we implement the TDDFT-NEGF-HEOM-WBL method and demonstrate its validity by applying it to a CNT-based device.

This paper is organized as follows. In Sec. II, NEGF-HEOM-WBL method is described in detail, and the combination between NEGF-HEOM-WBL and first-principles method is introduced in a practical numerical scheme. A numerical example on CNT-based device and discussion are given in Sec. III. Finally, a summary is given in Sec. IV.

II. TIME-DEPENDENT DENSITY FUNCTIONAL THEORY FOR OPEN ELECTRONIC SYSTEM

As TDDFT is an effective single-electron model, we confine ourselves to the effective single-electron Hamiltonian as follows:

$$H = H_D + \sum_\alpha [H_\alpha + H_{\alpha D}], \quad (1)$$

where H_D and H_α are the Hamiltonians of the device and lead α, respectively; $H_{\alpha D}$ is the interaction Hamiltonian between device and lead α. The Hamiltonian of the device region reads

$$H_D = \sum_{\mu\nu} h_{\mu\nu}(t) d_\mu^\dagger d_\nu, \quad (2)$$

where $d_\mu^\dagger$ and d_ν are the electronic creation and annihilation operators in the device region, respectively; $h_{\mu\nu}$ is the corresponding single-electron Fock matrix. For TDDFT, $h_{\mu\nu}$ is the Kohn-Sham (KS) Fock matrix which is obtained by projecting KS Fock operator onto a given set of basis. The Hamiltonian of lead α is $H_\alpha = \sum_k \epsilon_{k_\alpha}(t) c_{k_\alpha}^\dagger c_{k_\alpha}$, where $c_{k_\alpha}^\dagger$ and c_{k_α} are the electronic creation and annihilation operators in the lead α, respectively. $\epsilon_{k_\alpha}(t)$ is the single-particle energy, the time dependence of which comes from applied bias voltage. The variation of single-particle energy in lead α upon time-dependent bias is assumed to be $\epsilon_{k_\alpha}(t) = \epsilon_{k_\alpha}^0 + \Delta_\alpha(t)$, with $\Delta_\alpha(t)$ being the voltage applied on lead α. The interaction Hamiltonian between device and lead α reads $H_{\alpha D} = \sum_{\alpha k,\mu} (V_{k_\alpha \mu} c_{k_\alpha}^\dagger d_i + \text{H.c.})$, where $V_{k_\alpha \mu}$ is the coupling strength.

With the Hamiltonian described above, the EOM of the RSDM reads[1]

$$i\dot{\sigma}(t) = [h(t),\sigma(t)] - \sum_\alpha [\varphi_\alpha(t) - \varphi_\alpha^\dagger(t)], \quad (3)$$

in which the auxiliary density matrix $\varphi_\alpha(t)$ is expressed in terms of NEGF:

$$\varphi_\alpha(t) = i \int_{-\infty}^{t} d\tau [G^<(t,\tau)\Sigma_\alpha^>(\tau,t) - G^>(t,\tau)\Sigma_\alpha^<(\tau,t)], \quad (4)$$

 ©2013 American Physical Society

where $\alpha = L,R$. $G^<(t,\tau)$ and $G^>(t,\tau)$ are the lesser and greater Green's function of device, respectively. $\Sigma_\alpha^<(t,\tau)$ and $\Sigma_\alpha^>(t,\tau)$ are the lesser and greater self-energies due to the coupling between device and lead α, respectively. The lesser and greater self-energy can be expressed as[20]

$$\Sigma_\alpha^{<,>}(\tau,t) = \pm 2i \int \frac{d\epsilon}{2\pi} f_\alpha^\pm(\epsilon) e^{i\int_\tau^t [\epsilon+\Delta_\alpha(t_1)]dt_1} \Lambda_\alpha(\epsilon), \tag{5}$$

where $f_\alpha^\pm(\epsilon) = 1/(e^{\pm\beta(\epsilon-\mu_\alpha)}+1)$ is the Fermi distribution, with β being the inverse temperature. $\Lambda_\alpha(\epsilon)$ is the linewidth function and can be expressed as

$$[\Lambda_\alpha(\epsilon)]_{ij} = \pi \sum_{k_\alpha} \delta(\epsilon - \epsilon_{k_\alpha}) V_{k_\alpha,i}^* V_{k_\alpha,j}. \tag{6}$$

Equations (3) and (4) are the general formalism for open electronic systems coupled with noninteracting leads. Since $G^<(t,\tau)$ corresponds to the electron-density matrix $[G^<(t,t) = i\sigma(t)]$ and $G^>(t,\tau)$ corresponds to hole density matrix $\{G^>(t,t) = -i[1-\sigma(t)]\}$, the first term of Eq. (4) is interpreted as the outcoming rate of electron from device to lead α. Similarly, the second term of Eq. (4) is interpreted as the incoming rate of electron from lead α to device. Hence, $\varphi_\alpha(t)$ corresponds to the net rate of electron going through the interface between lead α and device, and the transient current can be evaluated by taking the trace of the auxiliary density matrix $\varphi_\alpha(t)$:

$$I_\alpha(t) = i\mathrm{Tr}[\varphi_\alpha(t) - \varphi_\alpha^\dagger(t)]. \tag{7}$$

The RSDM can be solved by performing time-domain propagation of Eq. (3). The complexity now lies in the evaluation of the auxiliary density matrix $\varphi_\alpha(t)$. In order to implement this method to simulate realistic systems from first-principles, an efficient method to deal with $\varphi_\alpha(t)$ is desirable. To achieve this, the WBL approximation is employed, which involves the following assumptions for the leads: (i) bandwidths are assumed to be infinitely large; (ii) linewidths are assumed to be energy independent, i.e., $\Lambda_\alpha(\epsilon) = \Lambda_\alpha$. Within the WBL approximation, the self-energy becomes

$$\Sigma_\alpha^{<,>}(\tau,t) = \pm 2i \int \frac{d\epsilon}{2\pi} f_\alpha^\pm(\epsilon) e^{i\int_\tau^t [\epsilon+\Delta_\alpha(t_1)]dt_1} \Lambda_\alpha, \tag{8}$$

where $\Lambda_\alpha = \pi \sum_{k_\alpha} |V|^2 \delta(\epsilon_f - \epsilon_{k_\alpha})$ is the linewidth function evaluated at Fermi energy ϵ_f of the unbiased system. To further enhance the calculation efficiency, Padé approximation is applied, in which the Fermi distribution function is expanded as[21]

$$f_\alpha^\pm(\epsilon) \approx \frac{1}{2} \mp \sum_k^N \left[\frac{\eta_k}{\beta(\epsilon-\mu_\alpha)+i\zeta_k} + \frac{\eta_k}{\beta(\epsilon-\mu_\alpha)-i\zeta_k} \right], \tag{9}$$

where $\pm i\zeta_k/\beta + \mu_\alpha$ are the kth Padé poles in the upper and lower half plane, respectively; η_k/β is the corresponding coefficient. The accuracy of Padé expansion is determined by the expansion order. Take $f_\alpha^+(\epsilon)$ for example, its deviation from the exact Fermi distribution function is defined as $\delta f_\alpha(\epsilon)$. Since $\delta f(\epsilon)$ is an odd and monotonic increasing function respect to $\beta(\epsilon - \mu_\alpha)$, only the domain of $\beta(\epsilon-\mu_\alpha) > 0$ needs to be examined. In this region, $\delta f(\epsilon)$ increases from 0 to $\frac{1}{2}$ monotonically. A validity L is defined as $\delta f(\epsilon)|_{\beta(\epsilon-\mu_\alpha)=L} = \delta$, where δ is the tolerance desired in the simulation. It is easy to show that the validity length L is dependent on expansion order N. Take $\delta = 10^{-7}$ for instance, the relation between the validity length L and the expansion order N is shown in Fig. 1.

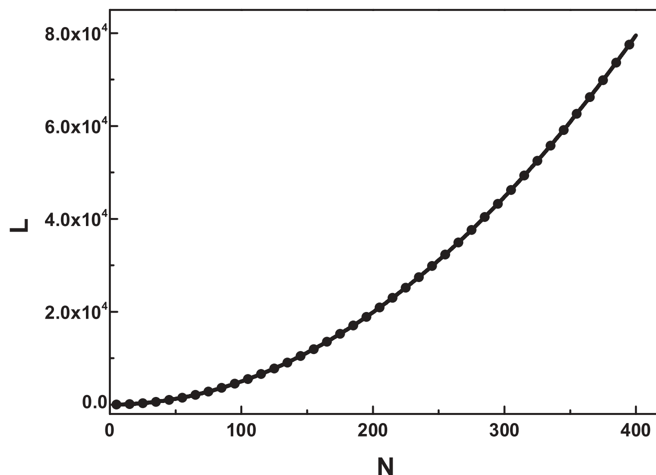

FIG. 1. Validity length L of Padé expansion against expansion order N.

For a certain system at temperature T, the number of Padé expansion needed is determined by searching for an N whose corresponding validity length is equal to $\beta(\epsilon_{\max} + |\mu_\alpha|)$, where $\epsilon_{\max}$ is the maximum absolute value of the eigenvalues of Fock matrix. Figure 1 indicates that higher-order Padé expansion is needed for the system with lower temperature or larger energy scale.

Based on Padé expansion and WBL approximation, the integration in Eq. (8) can be evaluated analytically through contour integration and residue theorem; the resulting expression of self-energy is

$$\Sigma_\alpha^{<,>}(\tau,t) \approx \pm \frac{i}{2}\delta(t-\tau)\Lambda_\alpha + x\sum_k^N \Sigma_{\alpha k}^x(\tau,t), \tag{10}$$

where $x = +$ for $t \geqslant \tau$ and $x = -$ for $t < \tau$. The sign x corresponds to upper (+) or lower half plane (−) contour integration. $\Sigma_{\alpha k}^\pm(\tau,t)$ is defined as

$$\Sigma_{\alpha k}^\pm(\tau,t) = \frac{2}{\beta}\eta_k e^{i\int_\tau^t \epsilon_{\alpha k}^\pm(t_1)dt_1} \Lambda_\alpha, \tag{11}$$

where $\epsilon_{\alpha k}^\pm(t) = \pm i\zeta_k/\beta + \mu_\alpha + \Delta_\alpha(t)$. Based on the approximation on self-energy described in Eq. (10), the auxiliary density matrix is rewritten as

$$\varphi_\alpha(t) = i[\sigma(t) - 1/2]\Lambda_\alpha + \sum_k^N \varphi_{\alpha k}(t). \tag{12}$$

The first term on the right-hand side (RHS) of the above equation comes from the integration over lesser/greater Green's function and δ function, and the second term on the RHS of Eq. (12) is

$$\varphi_{\alpha k}(t) = -i\int_{-\infty}^{\infty} d\tau G^r(t,\tau)\Sigma_{\alpha k}^+(\tau,t), \tag{13}$$

where $\varphi_{\alpha k}(t)$ is the component of the first-tier auxiliary density matrix, which is evaluated through its EOM. Within the WBL approximation, the EOMs of $G^r(t,\tau)$ and $\Sigma^+_{\alpha k}(\tau,t)$ are linear equations of themselves. Therefore, it is straightforward to write down the EOM of the first-tier auxiliary density matrix as

$$i\dot{\varphi}_{\alpha k}(t) = -\frac{2i\eta_k}{\beta}\Lambda_\alpha - [\epsilon^+_{\alpha k}(t) - h(t) + i\Lambda]\varphi_{\alpha k}(t), \tag{14}$$

where $\Lambda = \sum_\alpha \Lambda_\alpha$ is the total linewidth function. Hence, Eqs. (3), (12), and (14) constitute a close set of EOMs, which provides a practical and efficient NEGF-HEOM-WBL scheme for simulating the transient dynamics of noninteracting systems. Solutions to the density matrix and auxiliary density matrix are evaluated through these three equations with corresponding initial conditions.

At initial time $t = 0$, the system is in its equilibrium state, in which all the quantities are time independent. Hence, the time derivative of the density matrix and auxiliary density matrices are zero. From Eq. (14), it is straightforward to write down the initial condition for auxiliary density matrix $\varphi_{\alpha k}(0)$ as

$$\varphi_{\alpha k}(0) = -\frac{2i\eta_k}{\beta}\frac{1}{\epsilon_{\alpha k}(0) - h(0) + i\Lambda}\Lambda_\alpha. \tag{15}$$

Then $\varphi_\alpha(0)$ can be obtained from Eq. (12). The EOM of the density matrix $\sigma(0)$, i.e., Eq. (3), reduces to a nonlinear equation for itself. It can be evaluated by employing the NEGF method as

$$\sigma(0) = \frac{1}{2}\mathbf{I} + \sum_{\alpha k}\mathrm{Re}\frac{2\eta_k}{\beta}\frac{1}{\epsilon_{\alpha k}(0) - h(0) + i\Lambda}. \tag{16}$$

Equations (15) and (16) provide the initial conditions for solving the density matrix and auxiliary density matrix. After bias voltage is switched on, the device is driven out of equilibrium. The dynamic response of the device is obtained by solving EOM of $\sigma(t)$ and $\varphi_{\alpha k}(t)$ in time domain.

The NEGF-HEOM-WBL formalism has been implemented in the framework of TDDFT and time-dependent density functional tight-binding (TDDFTB) method,[16,22] namely TDDFT(B)-NEGF-HEOM-WBL. DFTB is an approximated DFT based on the second-order expansion of DFT KS energy respect to charge density fluctuations on a reference system. Within TDDFT(B)-NEGF-HEOM-WBL formalism, the system is assumed to be in its ground state initially, the properties of which are determined by molecular cluster based technique.[1] The extended cluster contains not only the device region but also the portions of leads, since the calculation of linewidth function $\Lambda_{L/R}$ depends on device-lead coupling matrix $V_{k_\alpha\mu}$ which is off-diagonal block of the extended cluster's KS Fock matrix. When the ground state of the extended cluster is obtained, diagonal blocks of the ground-state KS Fock matrix corresponding to leads are extracted to evaluate the surface Green's function $g^r_{L/R}$.[23] Then the off-diagonal blocks corresponding to the coupling between device and leads are extracted to construct the linewidth function $\Lambda_{L/R}$ within the WBL approximation, i.e., $\Lambda_{ij}(\epsilon_f) = \pi\sum_{k_\alpha} V^*_{k_\alpha,i} g^r_{k_\alpha}(\epsilon_f) V_{k_\alpha,j}$. With those quantities known, initial conditions for density matrix and auxiliary density matrix are obtained as described above.

After bias voltage is turned on, Hartree potential $V_H(\mathbf{r},t)$ and exchange correlation (XC) potential $V_{xc}(\mathbf{r},t)$ are updated according to the change of the electron density $\delta n(\mathbf{r},t)$ due to bias voltage applied at the leads. Therefore, the change of the KS Fock matrix induced by bias voltage includes Hartree and XC components, i.e.,

$$h(t) = h(0) + \delta V_H(t) + \delta V_{xc}(t), \tag{17}$$

where $h(0)$ is the ground-state KS Fock matrix. $\delta V_H(t)$ and $\delta V_{xc}(t)$ are obtained by projecting bias induced Hartree potential $\delta V_H(\mathbf{r},t)$ and XC potential $\delta V_{xc}(t)$ on atomic basis set, respectively. $\delta V_{xc}(\mathbf{r},t)$ is evaluated from the change of electron density $\delta n(\mathbf{r},t)$. In this work, adiabatic local-density approximation (ALDA) is adopted for XC functional. The Hartree potential $\delta V_H(\mathbf{r},t)$ can be evaluated from the Poisson equation,

$$\nabla^2 \delta V_H(\mathbf{r},t) = -4\pi\delta n(\mathbf{r},t), \tag{18}$$

which is subject to the boundary condition,

$$\begin{aligned} \delta V_H(\mathbf{r},t)|_{S_L} &= V_L(t), \\ \delta V_H(\mathbf{r},t)|_{S_R} &= V_R(t), \end{aligned} \tag{19}$$

where S_L/S_R are the the interfaces between device and leads; $V_{L/R}(t)$ is the bias voltage applied on lead L/R.

The time propagation of the density matrix $\sigma(t)$ and auxiliary density matrix $\varphi_{\alpha k}(t)$ are evaluated by employing the fourth-order Runge-Kutta (RK4) method. Transient current at each time step is obtained from Eq. (7). The number of auxiliary density matrix is determined by the truncation of Padé expansion. For instance, suppose Padé expansion is truncated at N_kth order, there will be $2N_k$ $\varphi_{\alpha k}(t)$ matrices to be evaluated from the EOMs at each time step. This is the most time-consuming part. However, the linewidth function Λ_α is a sparse matrix, especially for a large system where only a small part of Λ_α have nonzero values. As a result, only a small block of Λ_α and partial block of $\varphi_{\alpha k}(t)$ are needed to be calculated in the numerical implementation, which greatly reduces the computational costs and makes it possible to simulate large systems.

III. NUMERICAL RESULT AND DISCUSSION

To illustrate the validity of this method, a comparison between the WBL and non-WBL simulation is carried out on a model system. The details about the non-WBL time-dependent transport method is described in Ref. 14. The model system contains a single energy level coupled to two leads, onsite energy is set to be $\epsilon_0 = 0$ eV. For the non-WBL method, the linewidth function is described as a single Lorentzian function $\Lambda_\alpha(\epsilon) = \Gamma^0_\alpha W^2/(\epsilon^2 + W^2)$, where W is the width of Lorentzian function. For the WBL method, the linewidth function is set to be $\Lambda_\alpha(0) = \Gamma^0_\alpha$, i.e., the value when the width of the Lorentzain linewidth function approaches infinity, $W \sim \infty$. With bias voltage switched on at $t = 0$, the shift of onsite energy is set as $\epsilon(t) = \epsilon_0 + [V_L(t) + V_R(t)]/2$.

In the numerical calculations, parameters are set as follows: $\Gamma^0_L = \Gamma^0_R = 0.25\Gamma$; the width of Lorentizan linewidth function $W = 20\Gamma$; bias voltages $V_R = 0$, $V_L = 5\Gamma$; temperature is set to be $K_BT = 0.1\Gamma$. Transient currents obtained from both the WBL and non-WBL method are shown in Fig. 2, which reveals that the two results agree quantitatively with each other.

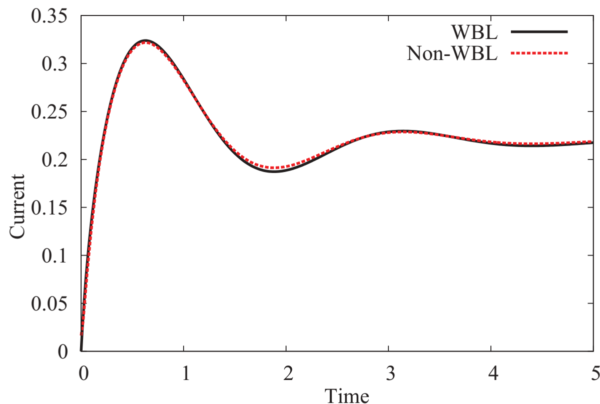

FIG. 2. (Color online) Transient current of single site system with WBL approximation (solid line) and non-WBL (dash line). Time is in units of $\hbar/\Gamma$, current is in units of $e\Gamma/\hbar$. See text for parameters.

The reason is that the system under investigated is in linear response region, since the applied bias voltage is much smaller than the width of the Lorentzian linewidth function. As a result, the accuracy for the applying of WBL approximation is guaranteed, hence the two results perfectly match. The results also verify that WBL is a reasonable approximation in the linear response region. In such region, it is appropriate to use the WBL method to simulate the transient current of the realistic system.

Next, a first-principles simulation is carried out on a (5, 5) CNT-based device. As shown in Fig. 3, the (5, 5) CNT contains 60 carbon atoms, and is connected to aluminum leads at each side. The distance between the CNT and the aluminum lead is 1.5 Å. Each unit cell of aluminum contains 16 atoms, and one unit cell of the lead on each side is included in the device region. The whole device region contains 60 carbon atoms and 32 aluminum atoms.

For the CNT-based device described above, comparisons between the WBL and AWBL methods are made. Since the AWBL method is applicable for zero temperature, the WBL simulation is carried out at very low temperatures (5 K in this case) in order to make the comparison more meaningful. The largest absolute value of the eigenvalues of Fock matrix is around 19 eV after the core orbitals are excluded through a projector operator,[24] which requires the validity length of the Padé expansion to be at least 4.4×10^4. As a result, 300 order Padé expansion is used for the WBL simulation to acheive tolerance $\delta = 10^{-7}$ according to Fig. 1. The two methods are carried out in both TDDFT and TDDFTB schemes with time step for the RK4 propagation being 0.015 fs. The minimal basis set STO-3G is chosen in the TDDFT simulation.

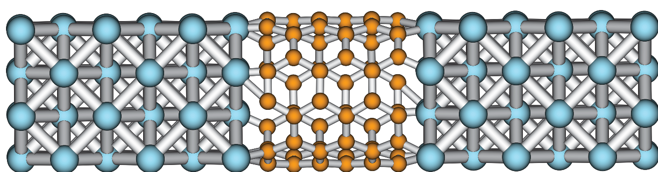

FIG. 3. (Color online) CNT-based device. There are 60 atoms for the (5, 5) CNT and 16 atoms in a unit cell of aluminum leads.

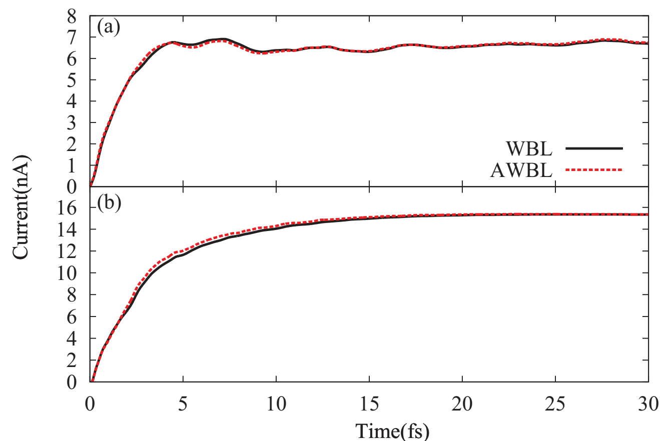

FIG. 4. (Color online) Transient current corresponding to exponential growth bias voltage. (a) TDDFT; (b) TDDFTB. See text for parameters.

Figure 4 shows the transient currents induced by exponential growth bias voltage for both TDDFT and TDDFTB simulations. The applied bias voltage is $V(t) = V_0(1 - e^{-t/a})$, where $V_0 = 0.1$ meV and $a = 1$ fs. As shown in Fig. 4, the transient response to the bias voltage is very fast. The current almost approaches its steady state in 10 fs. For exponential growth bias voltage, the transient currents calculated by the two methods agree quite well with each other except a slight difference at the beginning, where the voltage changes dramatically shortly after being switched on. The difference is due to the fact that AWBL is not able to capture all the memory effect as exactly as WBL. However, when the system is approaching its steady state, the fluctuation becomes smaller and smaller in the long-time limit, making the memory effect less significant.

For ac transport cases, the applied bias voltage is periodic in time and always drives the system out of steady state. As a result, memory effect plays a more important role than that for exponential growth bias voltage. Figures 5 and 6 show the transient currents obtained from TDDFT and TDDFTB

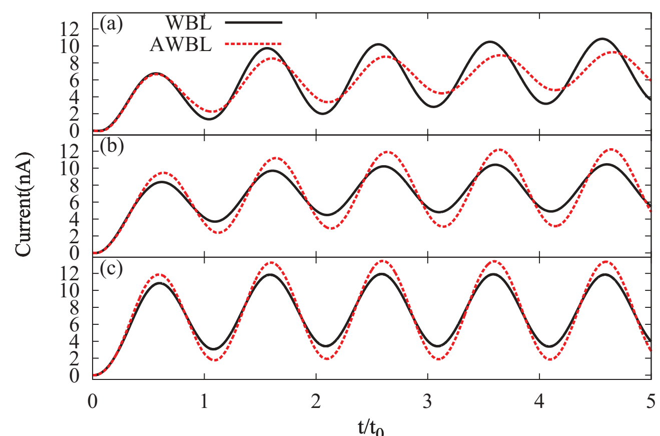

FIG. 5. (Color online) TDDFT calculation of transient current corresponding to sinusoidal bias voltage, $V(t) = \frac{V_0}{2}[1 - \cos(\frac{2\pi t}{t_0})]$, $V_0 = 0.1$ meV. (a) $t_0 = 2$ fs; (b) $t_0 = 5$ fs; (c) $t_0 = 10$ fs. The black solid line is WBL current; red dashed line is AWBL current.

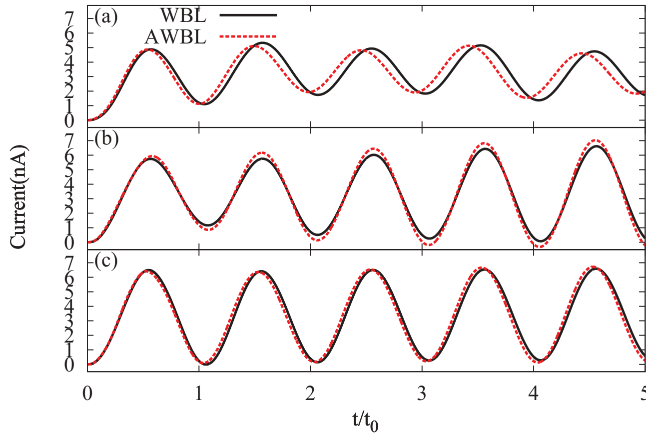

FIG. 6. (Color online) TDDFTB simulation of transient current corresponding to sinusoidal bias voltage, $V(t) = \frac{V_0}{2}[1 - \cos(\frac{2\pi t}{t_0})]$, $V_0 = 0.1$ meV. (a) $t_0 = 2$ fs; (b) $t_0 = 5$ fs; (c) $t_0 = 10$ fs. The black solid line is WBL current; red dashed line is AWBL current.

simulations under sinusoidal bias voltages, respectively. For both TDDFT and TDDFTB simulations, the AWBL and WBL methods show different phase delays, especially for high-frequency bias. For instance, in the case of TDDFTB simulation under high-frequency bias ($t_0 = 2$ fs), the phase of the AWBL current is even ahead of that of the bias voltage. By comparing (a), (b), and (c) in Figs. 5 and 6, it can be found that WBL is more suitable for high-frequency response. However, when low-frequency ac bias voltage is applied, the two methods agree well with each other. This result indicates that AWBL is good enough for ac conductance simulations at low frequency, while WBL method should be used if ac conductance for high frequency is desired.

It should be pointed out that both the AWBL and WBL methods are numerically efficient compared to the conventional NEGF formula which directly discretizes the time.[13] Figure 7(a) shows the relationship between the CPU time and the simulated time, which is obtained through TDDFT-NEGF-HEOM-WBL calculation on a CNT-based device. While the relationship between the CPU time and the number of atoms is shown in Fig. 7(b), which is obtained through TDDFT-NEGF-HEOM-WBL calculation on a carbon chain. A carbon chain is selected because only a small number of atoms are contained in one unit cell, making it more flexible for the scaling calculation of CPU time. The simulation in Fig. 7(b) is fixed at 0.15 fs, i.e., ten time steps. Since the density matrix and auxiliary density matrix are solved through EOMs with the RK4 method, the CPU time is proportional to the simulated time, which is confirmed by Fig. 7(a). As shown in Fig. 7(b), since the time complexity of matrix multiplication is $O(N^3)$ (N is the number of atoms), the CPU time scales as $O(N^3)$ against the number of atoms.

IV. SUMMARY

In this work, an efficient first-principles method for time-dependent quantum transport at finite temperature is proposed at the level of WBL approximation for leads-device coupling. This formalism enables the transient simulation on large realistic systems at finite temperature corresponding to

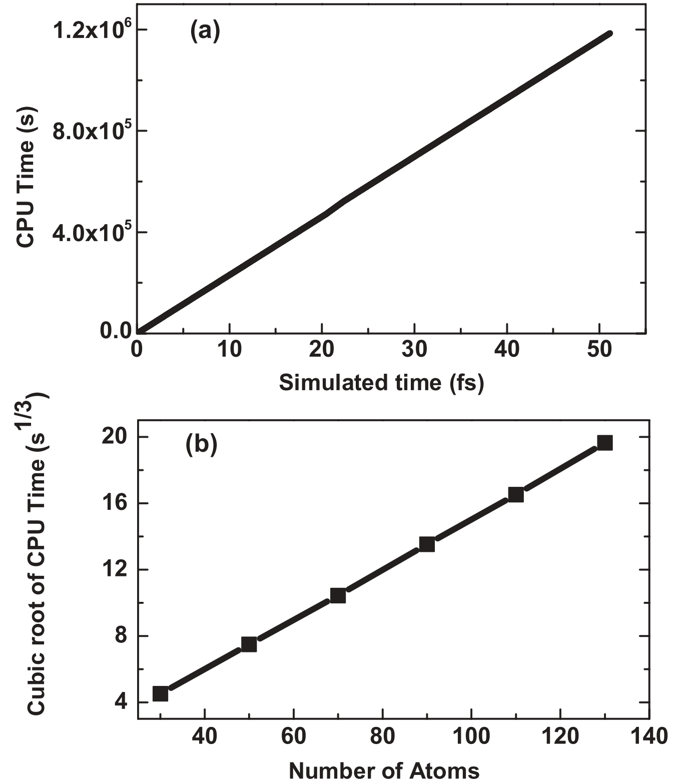

FIG. 7. CPU time against simulated time and number of atoms. (a) Linear scaling of CPU time versus the simulated time; (b) CPU time scales as $O(N^3)$ against number of atoms N.

arbitrary bias voltages and is implemented with both TDDFT and TDDFTB. The performance of the TDDFT(B)-NEGF-HEOM-WBL is demonstrated via the numerical simulation on CNT-based device. The CPU time scales linearly against simulated time and scales as $O(N^3)$ against the number of atoms N. The computational cost of the newly developed TDDFT(B)-NEGF-HEOM-WBL method is mainly controlled by the first-tier auxiliary density matrix $\varphi_{\alpha k}(t)$ which depends on the number of Padé expansion. A lesser number of Padé expansion is needed for higher temperature, making this method especially suitable for room-temperature simulation. Besides, according to the sparsity of the first-tier auxiliary density matrix $\varphi_{\alpha k}(t)$, only a small block of $\varphi_{\alpha k}(t)$ needs to be evaluated, which reduces the computational cost of evaluating $\varphi_{\alpha k}(t)$. Another important result of this work is that the TDDFT-NEGF-AWBL is found to be quite accurate as long as the frequencies involved are not too high, which validates further the previous works.[1,19] As long as we are interested in the linear electric response region, the TDDFT(B)-NEGF-HEOM-WBL formalism developed here provides the accurate numerical results. Beyond the linear response region, the electronic structures of the electrodes need to be taken into account. Work along this direction is in progress.

ACKNOWLEDGMENTS

Support from the Hong Kong Research Grant Council (Contracts No. HKU7009/09P, No. 7009/12P, No. 7007/11P, and No. HKUST9/CRF/11G), and the University Grant Council (Contract No. AoE/P-04/08) is gratefully acknowledged.

*ghc@everest.hku.hk

[1] X. Zheng, F. Wang, C. Y. Yam, Y. Mo, and G. H. Chen, Phys. Rev. B **75**, 195127 (2007).

[2] M. Di Ventra and R. D'Agosta, Phys. Rev. Lett. **98**, 226403 (2007).

[3] R. D'Agosta and M. Di Ventra, Phys. Rev. B **78**, 165105 (2008).

[4] M. D. Ventra and T. N. Todorov, J. Phys.: Condens. Matter **16**, 8025 (2004).

[5] J. Yuen-Zhou, C. Rodriguez-Rosario, and A. Aspuru-Guzik, Phys. Chem. Chem. Phys. **11**, 4509 (2009).

[6] J. Yuen-Zhou, D. G. Tempel, C. A. Rodríguez-Rosario, and A. Aspuru-Guzik, Phys. Rev. Lett. **104**, 043001 (2010).

[7] D. G. Tempel, M. A. Watson, R. Olivares-Amaya, and A. Aspuru-Guzik, J. Chem. Phys. **134**, 074116 (2011).

[8] X. Zheng, C. Y. Yam, F. Wang, and G. H. Chen, Phys. Chem. Chem. Phys. **13**, 14358 (2011).

[9] E. Runge and E. K. U. Gross, Phys. Rev. Lett. **52**, 997 (1984).

[10] G. Stefanucci and C.-O. Almbladh, Phys. Rev. B **69**, 195318 (2004).

[11] S. Kurth, G. Stefanucci, C.-O. Almbladh, A. Rubio, and E. K. U. Gross, Phys. Rev. B **72**, 035308 (2005).

[12] X. Zheng, G. H. Chen, Y. Mo, S. Koo, H. Tian, C. Y. Yam, and Y. Yan, J. Chem. Phys. **133**, 114101 (2010).

[13] L. Zhang, Y. Xing, and J. Wang, Phys. Rev. B **86**, 155438 (2012).

[14] H. Xie, F. Jiang, H. Tian, X. Zheng, Y. Kwok, S. G. Chen, C. Y. Yam, Y. Yan, and G. H. Chen, J. Chem. Phys. **137**, 044113 (2012).

[15] E. Khosravi, A.-M. Uimonen, A. Stan, G. Stefanucci, S. Kurth, R. van Leeuwen, and E. K. U. Gross, Phys. Rev. B **85**, 075103 (2012).

[16] Y. Wang, C. Yam, T. Frauenheim, G. Chen, and T. Niehaus, Chem. Phys. **391**, 69 (2011).

[17] S. Kurth, G. Stefanucci, E. Khosravi, C. Verdozzi, and E. K. U. Gross, Phys. Rev. Lett. **104**, 236801 (2010).

[18] G. Vignale and W. Kohn, Phys. Rev. Lett. **77**, 2037 (1996).

[19] C. Y. Yam, Y. Mo, F. Wang, X. Li, G. H. Chen, X. Zheng, Y. Matsuda, J. Tahir-Kheli, and W. A. G. III, Nanotechnology **19**, 495203 (2008).

[20] A.-P. Jauho, N. S. Wingreen, and Y. Meir, Phys. Rev. B **50**, 5528 (1994).

[21] J. Hu, M. Luo, F. Jiang, R.-X. Xu, and Y. Yan, J. Chem. Phys. **134**, 244106 (2011).

[22] M. Elstner, D. Porezag, G. Jungnickel, J. Elsner, M. Haugk, T. Frauenheim, S. Suhai, and G. Seifert, Phys. Rev. B **58**, 7260 (1998).

[23] M. P. L. Sancho, J. M. L. Sancho, J. M. L. Sancho, and J. Rubio, J. Phys. F: Metal Physics **15**, 851 (1985).

[24] F. Wang, C. Y. Yam, G. Chen, and K. Fan, J. Chem. Phys. **126**, 134104 (2007).